Influence of Thermally Driven Surface Undulations on Tethers Formed from Bilayer Membranes

Emily Glassinger and Robert M. Raphael
Department of Bioengineering, Rice University, Houston, Texas

ABSTRACT Tether formation is a powerful method to study the mechanical properties of soft lipid bilayer membranes. The force required to maintain a tether at a given length depends upon both membrane elastic properties and tension. In this report, we develop a theoretical analysis that considers the contribution of thermally driven surface undulations and the corresponding entropically driven tensions on the conformation of tethers formed from unaspirated lipid vesicles. In this model, thermal undulations of the vesicle surface provide the excess area required for tether formation. Energy minimization demonstrates the dependence of equilibrium tether conformation on membrane tension and provides an analytical relationship between tether force and radius. If the contributions of nonlocal bending are not considered, an analytical relationship between tether force and length can also be obtained. The predictions of the model are compared to recently reported experimental data, and a value for the initial vesicle tension is obtained. Since most analyses of tether formation from cells and unaspirated vesicles neglect the contributions of nonlocal bending, the appropriateness of this assumption is analyzed. The effect of surface microvesiculations on the tether force-length relation is also considered.

INTRODUCTION

The formation and dynamics of tubular intracellular organelles such as the endoplasmic reticulum involve a coordinated interplay between a number of proteins, signaling intermediates and lipid species. Full understanding of how these membranous structures are formed relies in part on the characterization of the material properties of the membrane. The mechanical behavior of membranes drawn into a tubular shape can be studied by physically extracting bilayer tubes, termed tethers, from lipid membranes. In support of the proposed bilayer, tubular architecture of the tether, shape analyses indicate tethers are stable provided there is a finite tension (1). To form a tether, a silica or polystyrene bead is attached to the surface of a vesicle or cellular membrane and then pulled away from the surface. Often, tethers are extracted from vesicles aspirated into a micropipette. Aspiration stabilizes the vesicle and controls the elastic tension of the membrane. Not only have these tether experiments provided a new means to measure the local bending modulus k_c (2,3), but analyses of these experiments have helped to establish the area difference elasticity theory (2,4,5). According to this theory, bending a closed bilayer induces a differential area strain between the two membrane leaflets (6,7). Since the differential area strain is distributed over the entire membrane surface, this type of deformation is termed nonlocal bending. By considering the relaxation of the tether formation induced area difference over the entire vesicle surface, parameters such as the rate of intermonolayer flip-flop and the interleaflet drag coefficient can be measured (8–11).

Though many basic membrane properties can be characterized by pulling tethers from aspirated bilayers, tether experiments are often conducted on unaspirated membranes. In fact, tethers were first observed when red blood cells and neutrophils were exposed to fluid flow (12). Following the development of more recent tether formation methods, such as optical tweezers and fiber-deflection techniques, tether studies have helped characterize the membrane-cytoskeleton adhesion energy (13–16). Protrusive tether-like structures have been observed in several experiments which examine the interaction between cytoskeletal components and lipid membranes. As tubulin polymerizes inside of a vesicle, the biopolymers induce an axial tubular membrane protrusion with a geometry similar to a membrane tether (17,18). In addition, microtubule motor proteins can form tethers from lipid vesicles in vitro (19,20).

To understand the forces these molecules exert on lipid membranes, optical tweezers have been used to measure the force required to form tethers from both unaspirated lipid bilayers as well as from reconstituted Golgi and endoplasmic reticulum networks (20,21). Distinct from the aspirated case, a lateral tension is not imposed a priori on the membrane. As a result, tether studies can be conducted on membranes with tensions much lower than those induced by an aspiration pipette and more similar to those of many cellular membranes.

For a membrane under low tension, the thermally induced fluctuations of the vesicle surface are more pronounced than those of a membrane under moderate tension (22–24). Since the bending energy is on the order of kT, the fluctuations manifest as out-of-plane undulations of the vesicle surface (25). As a result, the total surface area of the membrane is greater than the apparent or measured surface area. This

Submitted June 9, 2005, and accepted for publication April 5, 2006.

Address reprint requests to Dr. Robert M. Raphael, Rice University, Dept. of Bioengineering, MS-142, PO Box 1892, Houston, TX 77251-1892. E-mail: rraphael@rice.edu.

0006-3495/06/07/619/07 $2.00

doi: 10.1529/biophysj.105.068270

''excess'' surface area influences the response of a lipid membrane to a mechanical deformation. Expansion of the membrane area, for example, smoothes the surface undulations (22). Because flattening of the surface reduces the entropy, a force is needed to increase the apparent surface area. Thus, smoothing the surface undulations leads to an increase in membrane tension. The relationship between applied tension and area expansion has been demonstrated by micropipette aspiration experiments. When a vesicle is first aspirated into a micropipette, an increase in the observable surface area is accompanied by a small increase in tension. Upon further aspiration, the tension increases linearly with the area dilation (22,26,27). The observed behavior correlates with theoretical predictions in which the first phase is dominated by smoothing of the surface undulations and the second by expansion of the area per lipid molecule (28). According to this theory, the mean-square amplitude of these fluctuations depends upon the effective vesicle tension.

The effective tension of a vesicle can be manipulated by altering the relative concentration of internal and external impermeable solutes (11). Because the osmotic pressure is typically greater than the pressures created by mechanical manipulation, the volume of the vesicle is assumed to remain constant during tether formation (29). Under the constraint of constant volume, excess surface area is required to form a tether. To provide this area for micropipette aspiration tether experiments, vesicles are usually transferred to a hypertonic medium before tether extraction (2,8,30). Theoretical studies have considered the shape and stability of tethers formed from both axially strained vesicles and from lipid reservoirs (1,29,31,32). In another model, the unbinding of a strongly adhered, tense vesicle from the surface provides area for tether formation (33). Approaches applied for cellular membranes and unaspirated vesicles model the membrane from which the tether is formed as a disc with a far-field tension σ (34). By approximating the tether geometry as a simple cylinder, the tether force is expressed in terms of σ and the tether length L_t: $F = 2\pi(2k_c\sigma)^{1/2} + 4\pi^2 k_r L_t/A_o$ where A_o is the area of the vesicle, and k_c and k_r are the local and nonlocal bending moduli, respectively (3,34). The tether radius R_t is determined by the membrane tension σ, where $R_t = (k_c/2\sigma)^{1/2}$. Thus, if the tension does not change as a tether is lengthened, then the tether radius should remain constant. Recent experiments, however, have demonstrated a decrease in tether radius with an increase in tether length, suggesting membrane tension increases as a tether is elongated (20).

Here we develop a model of tether formation from an unaspirated lipid vesicle which provides a quantitative relation between membrane tension and tether length. In this model, we consider how entropically driven tensions may influence tether conformation; therefore, this model allows characterization of tethers formed from membranes that are not elastically tense. Following the approach first presented by Božič et al. (4), the vesicle shape is parameterized by a simple geometrical model, and only significant contributions to the thermodynamic potential are considered (4). Energy minimization provides an analytical relation between the equilibrium pulling force and the tether radius. Since tether radii often cannot be measured directly, an analytical relation between tether force and length is obtained by excluding the contributions of the nonlocal bending energy. Given many analyses of tether experiments do not consider nonlocal bending, we have analyzed the appropriate bounds of this approximation.

MODEL

The essential geometry is represented by the tether length L_t, the tether radius R_t, and the mean vesicle radius R_v (Fig. 1). Because $R_t \ll R_v$, the tether volume is neglected and the total volume can be approximated by the volume of a sphere of radius R_v (4). When combined with the constant volume constraint ($V = V_o$), the vesicle radius becomes a constant.

The equilibrium tether conformation can be predicted from the minimum of the energy expression:

$$\Phi = H - FL_t, \tag{1}$$

where H is the Helmholtz free energy and F is the tether force (4). The Helmholtz energy is composed of three terms: the local bending energy, the nonlocal bending energy, and the energy required to smooth the thermal fluctuations:

$$H = \frac{1}{2}k_c\int(\bar{c} - c_o)^2 dA + \frac{1}{2}\frac{k_r}{A_o h^2}(\Delta A - \Delta A_o)^2 + \frac{AkT}{8\pi k_c}\sigma. \tag{2}$$

The first term of Eq. 2 is the local bending energy (7,35). The local bending modulus k_c represents both monolayers' resistance to bending; $\bar{c}$ is the sum of the two principal curvatures, and c_o is the initial curvature of the bilayer. Because the bending energy of the tether is at least several orders of magnitude greater than the bending energy of other vesicle regions, only the bending energy of the tether is included in the energy expression (4).

The second term of Eq. 2, the nonlocal bending energy, accounts for the relative expansion and compression of each monolayer. The constant k_r is the nonlocal bending modulus and h is the distance between the neutral surfaces of each monolayer (4,6,7,36). Here ΔA represents the relative area

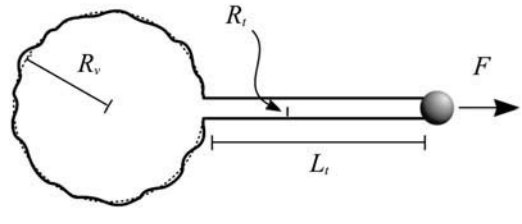

FIGURE 1 Geometric representation of tether formation by an applied force, F. The vesicle is depicted by a sphere of mean radius R_v and the tether by a cylinder of length L_t and radius R_t.

difference between the membrane leaflets; ΔA_o is included for completeness to account for the initial area difference between the monolayers. Using the expression $\int \bar{c} dA = \Delta A/h$, Eq. 2 may be rearranged so that the contributions of ΔA_o and c_o are grouped together into the reduced area difference ΔA_o^* and a constant w_o (5,37):

$$H = \frac{1}{2}k_c \int \bar{c}^2 dA + \frac{1}{2}\frac{k_r}{A_o h^2}(\Delta A - \Delta A_o^*)^2 + \frac{A_o kT}{8\pi k_c}\sigma + w_o, \quad (3)$$

where

$$\Delta A_o^* = \Delta A_o + \frac{k_c}{k_r} h A_o c_o$$

$$w_o = \frac{1}{2}k_c A_o c_o^2\left(1 - \frac{k_c}{k_r}\right) - \frac{\Delta A_o k_c c_o}{h}.$$

For this analysis, ΔA_o^* is taken to be zero; the consequences of a nonzero ΔA_o^* are considered in the Discussion. ΔA arising from tether formation is estimated from the difference between the areas of the inner tether leaflet, $2\pi L_t(R_t - h/2)$, and the outer leaflet, $2\pi L_t(R_t + h/2)$ (4).

The third term of Eq. 2 is the apparent area expansion energy, where σ is the effective membrane tension (25,38). The percent increase in measured area due to the flattening of the thermal fluctuations α is $(A_m - A_{m,o})/A_o$, where A_m is the measured area, $A_{m,o}$ is the initial measured area, and A_o is the total vesicle area (22). Because expansion of molecular area is not considered, the total area is held constant. Using a planar wave approximation for thermal fluctuations (22,25), the percent change in measured area is estimated as:

$$\alpha = \frac{kT}{8\pi k_c}\ln\left(\frac{\frac{\pi^2 k_c}{A_o} + \sigma}{\frac{\pi^2 k_c}{A_o} + \sigma_o}\right), \quad (4)$$

where σ_o is the initial effective membrane tension. This approximation is valid for $\sigma \ll \pi^2 k_c/a^2$; the constant a is the molecular spacing ($a \sim 5$ Å). For the geometry of this model, the change in measured area is

$$\alpha = \frac{4\pi R_v^2 + 2\pi R_t L_t - 4\pi R_{v,o}^2}{A_o}. \quad (5)$$

For a fixed volume ($V = V_o$; $R_v = R_{v,o}$), α reduces to $2\pi R_t L_t/A_o$. When the geometric and energetic approximations are applied, Eq. 1 becomes:

$$\Phi = \frac{A_o kT}{8\pi k_c}\left(\sigma_o + \frac{\pi^2 k_c}{A_o}\right)e^{\frac{16\pi^2 R_t L_t}{kTA_o}} + \pi k_c \frac{L_t}{R_t} + \frac{2\pi^2 k_r}{A_o}(L_t - L_t^*)^2 - FL_t + x_o, \quad (6)$$

where $L_t^* = \Delta A_o^*/2\pi h$. The constant x_o is $w_o - \pi kT/8$. By selecting a characteristic length scale as the radius of a sphere of area A_o and energy scale as the bending energy of a sphere ($8\pi k_c$), Eq. 6 can be written in nondimensional form in terms of the variables l_t and r_t ($l_t = L_t/R$; $r_t = R_t/R$):

$$\tilde{\Phi} = \frac{kT}{16\pi k_c}\left(\frac{\sigma_o R^2}{k_c} + \frac{\pi}{4}\right)e^{\frac{4\pi k_c r_t l_t}{kT}} + \frac{1}{8}\frac{l_t}{r_t} + \frac{1}{16}\frac{k_r}{k_c}(l_t - l_t^*)^2 - \mathcal{F} l_t + \mathcal{X}_o. \quad (7)$$

Here, the nondimensional force $\mathcal{F}$ is $FR/(8\pi k_c)$, and the initial tension $\mathcal{T}_o$ is $\sigma_o R^2/k_c$. At equilibrium, the partial derivatives of Eq. 7 are zero [$\partial\tilde{\Phi} = \partial\tilde{\Phi}(r_t, l_t) = 0$]. This provides two equations which can be solved to determine the minimum energy tether conformations:

$$\frac{\partial\tilde{\Phi}}{\partial l_t} = \frac{r_t}{4}\left(\frac{\sigma_o R^2}{k_c} + \frac{\pi}{4}\right)e^{\frac{4\pi k_c r_t l_t}{kT}} + \frac{1}{8r_t} + \frac{1}{8}\frac{k_r}{k_c}(l_t - l_t^*) - \mathcal{F} \quad (8)$$

and

$$\frac{\partial\tilde{\Phi}}{\partial r_t} = \frac{l_t}{4}\left(\frac{\sigma_o R^2}{k_c} + \frac{\pi}{4}\right)e^{\frac{4\pi k_c r_t l_t}{kT}} - \frac{1}{8}\frac{l_t}{r_t^2}. \quad (9)$$

The tether force equation, obtained by combining the dimensional forms of Eqs. 8 and 9, mirrors the equations derived by previous energy variational and force balance methods (3,4):

$$F = \frac{2\pi k_c}{R_t} + \frac{4\pi^2 k_r}{A_o}(L_t - L_t^*). \quad (10)$$

The constant L_t^* contributes to the total force. The difference between this model and those for aspirated vesicles, however, lies in the relation between L_r and R_t. This difference can be examined by solving Eq. 9 for L_t:

$$L_t = \frac{a}{R_t}\ln\left(\frac{b}{R_t^2}\right), \quad (11)$$

where $a = kTA_o/16\pi^2 k_c$ and $b = k_c/(2\sigma_o + 2\pi^2 k_c/A_o)$. Note that the relationship between L_t and R_t is independent of the nonlocal bending stiffness k_r.

RESULTS AND DISCUSSION

The solutions to Eqs. 8 and 9 predict that the initial effective vesicle tension influences tether conformation and that the membrane tension increases as the tether is lengthened (Fig. 2). The theoretical force required to maintain a tether of a given length decreases if the total surface area is increased or if the bending moduli are decreased. For example, for a vesicle in which $R = 10$ μm, $k_c = 5 \times 10^{-20}$ J, and a ratio of $k_r/k_c = 3$, the increase in force for a tether elongated from 5 to 15 μm is <1 pN. For a vesicle with a bending stiffness of 1×10^{-19} J, the increase in force is $\sim$5 pN. The membrane tension for a specified tether length depends upon the value of the initial tension (Fig. 2 *B*). If the initial vesicle tension is changed by an order of magnitude, the change in the force versus tether length curve is within experimental resolution (Fig. 2 *A*). These trends are significant as they motivate a method to determine the initial tension of a vesicle and

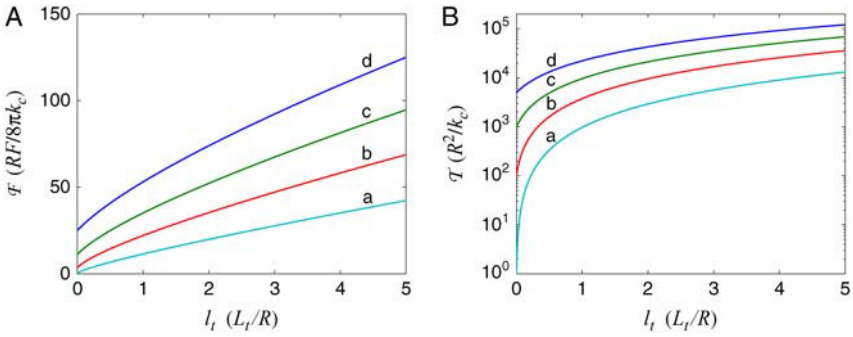

FIGURE 2 Calculated influence of initial tension on tether conformation. The initial values of $\mathcal{T}$ are (*b*) 100, (*c*) 1×10^3, and (*d*) 5×10^3 ($\mathcal{T}_o = \sigma_o R^2/k_c$). The special case (*a*) where $T = 0$ is included as a lower bound. These curves are plotted using typical mechanical moduli ($k_c = 1.0 \times 10^{-19}$ J and $k_r = 3.0 \times 10^{-19}$ J (8)).

indicate that even relatively small tensions influence tether behavior.

As an example of an application of this analysis, Eq. 11 is fit to previously reported data of tether formation from a 1,2 dioleoyl-*sn*-glycero-3-phosphocholine (DOPC) vesicle containing cholesterol and streptolysin O (SLO) (20) (Fig. 3 *A*). This is a unique case because SLO porates the membrane and thus lowers membrane tension. Due to the lowered tension, the tether radii can be measured using conventional light microscopy. We note, however, that since SLO porates the membrane, the vesicle volume may change (39). If volume changes with tether formation, then tether formation may simply lead to a decrease in the vesicle radius without affecting the extent of the thermal undulations. If the extent of the undulations is not altered, then the membrane tension should not change. However, as reported by Koster et al., when the tether is elongated, the tether radius decreases, indicating membrane tension increases with tether length (20). We stress that for this case, the analysis and the results from the fit serve only as a first order approximation.

Tether radii are usually too small to be resolved optically. Consequently, a relationship between F and L_t would aid in the interpretation of these experiments. An analytical expression of tether length as a function of tether force can be obtained by excluding the nonlocal bending term from Eq. 6. For short tether lengths (< 50 μm), the nonlocal bending energy is generally small and its contributions to tether equilibrium are often not considered in tether analyses (20,40). Under this assumption, Eq. 10 may be simplified to $F = 2\pi k_c/R_t$ and substituted into Eq. 11 to provide a relationship between the tether force and length:

$$L_t = cF \ln\left(\frac{F^2}{d}\right), \tag{12}$$

where $c = kTA_o/32\pi^3 k_c^2$ and $d = 8\pi^2 k_c(\sigma_o + \pi^2 k_c/A_o)$. A fit of Eq. 12 to the F versus L_t tether behavior for the SLO DOPC vesicle (20) is given in Fig. 3 *B*. Using the value of k_c reported for this vesicle (5.5×10^{-20} J), the calculated values of A_o and σ_o obtained from parameters c and d are 1.1×10^{-8} m^2 and 7.2×10^{-5} mN/m, respectively. These values are similar to those calculated from a fit of the R_t versus L_t data to Eq. 11: 1.2×10^{-8} m^2 and 8.2×10^{-5} mN/m (Fig. 3 *A*).

Since Eq. 12 was obtained by excluding the contributions of the nonlocal bending energy, we have analyzed the appropriateness of this assumption. The extent to which the energy affects equilibrium tether conformation depends upon the magnitude of the nonlocal bending coefficient k_r, the total vesicle area and the initial tension difference between the two membrane leaflets. The percent contribution of the nonlocal bending energy to the tether force is plotted for a range of tether lengths and ratios of k_r/k_c (Fig. 4). For a typical ratio of k_r/k_c (3.0 (2,8)), the percent contribution to the force for a tether in which $l_t = 4$ is <5%. The reported bending stiffness (5.5×10^{-20} J) used to obtain the fits in Fig. 3 was obtained from the slope of the experimentally measured plot F vs. $2\pi/R_t$ (20). Provided the initial area

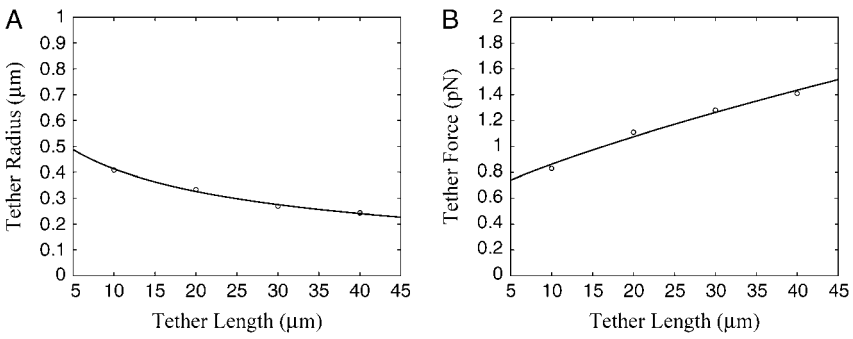

FIGURE 3 Fit of Eqs. 11 and 12 to experimental values reported by Koster et al. (20). The fits were calculated using a Levenberg-Marquardt algorithm. The parameter values obtained from the fits to the tether force (*A*) and radius (*B*) are: $a = 5.1 \pm 1.8 \times 10^{-12}$ m; $b = 3.8 \pm 2.2 \times 10^{-13}$ m^2; $c = 1.6 \pm 0.76 \times 10^7$ m/N; and $d = 2.8 \pm 1.9 \times 10^{24}$ N^2 (r^2: Plot *A*, 0.99; Plot *B*, 0.98). Although the tension values calculated from these parameters are similar to each other and within an expected range, we note the values are obtained from two parameter fits to four data points. This likely leads to the widths of the reported 90% confidence intervals.

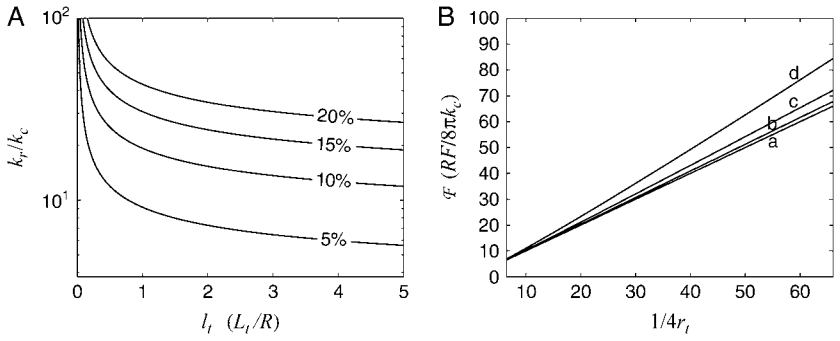

FIGURE 4 Influence of the nonlocal bending energy on the tether force. (*A*) The isolines represent the percent contribution of nonlocal bending to $\mathcal{F}$. This percent contribution to the tether force expressed in nondimensional form is $(k_r l_t/8k_c)/F$ and in dimensional form is $(4\pi^2 k_r L_t/A_o)/F$. (*B*) Nonlocal bending increases the force required to form a tether of a given radius. Note, $1/4r_t$ is the nondimensional form of the tether force equation that does not account for the nonlocal bending energy. The dimensional form is $2\pi k_c/R_t$. The ratios of k_r/k_c graphed in *B* are (*a*) 0, (*b*) 3, (*c*) 10, and (*d*) 30. Both *A* and *B* are plotted for a vesicle in which $k_c = 10^{-19}$ J, and $T = 31.8$.

difference between the membrane leaflets is negligible, nonlocal bending increases the slope of the plot of F vs. $1/4r$ (Fig. 4 *B*). Although neglecting the nonlocal bending energy may lead to an overestimation of the bending stiffness k_c, for a typical ratio of k_r/k_c of 3, the change in slope is $<5\%$ ($\sim 4\%$).

Both the relative initial area difference and the spontaneous curvature also contribute to the nonlocal bending energy. The contributions of both terms are encompassed by the constant L_t^*. Recall $L_t^* = \Delta A_o^*/2\pi h$. For a stable shape of the area difference elasticity model, ΔA_o^* can be related to the effective curvature, C_o^*: $\Delta A_o^* = C_o^* A_o h k_c/k_r$, where the effective curvature is given by $C_o^* = C_o + k_r/k_c(\Delta A_o/A_o h)$ (41). Hence, L_t^* may be expressed as $C_o^* A_o k_c/2\pi k_r$. Including this expression for L_t^* into Eq. 10 shifts the mechanical tether force by $2\pi C_o^* k_c$ (and F by $c_o^*/4$, where $c_o^* = RC_o^*$). Note that the effective spontaneous curvature depends not only upon the vesicle composition, formation, and history but also upon its aqueous bathing environment. Values of c_o^* for vesicles suspended in an asymmetric glucose solution, for example, range in value from ~ 2 to 6 (42). This shift may affect the behavior for vesicles under very low tensions such as described by curve *a* in Fig. 2 *A*. From Eq. 10, L_t^* provides a constant shift of the force; however, it does not change the slope of the relation between F and $1/r_t$. Since the slope reflects the value of k_c, neither the initial curvature nor the initial area difference affects this measurement of k_c.

The results obtained from this analysis can help to probe the microarchitecture of bilayer membranes. Experimental evidence indicates some vesicles contain surface microvesiculations that are not fully resolvable optically (41). The propensity to form these vesiculations may in part be due to the lipid composition of the vesicle. For example, under thermal expansion, the mean-square fluctuation amplitude of DMPC vesicles increases, whereas for SOPC vesicles microvesiculations form (41). Many cellular membranes also exhibit a rich spectrum of microarchitectural contours. Since a typical tether ($L_t = 10$ μm and $R_t = 100$ nm) formed from a vesicle in which $R = 10$ μm encompasses $\sim 0.5\%$ of the total vesicle area, microvesiculations could conceivably serve as an area reservoir for tether formation. To estimate the resulting tether behavior, we consider the simplest theoretical case in which area extraction from this reservoir occurs under constant membrane tension. For this case, the tether force equation provided in the introduction is applicable. As the tether is lengthened, the radius would remain constant and the force would increase slightly with the slope of $4\pi^2 k_r/A_o$. This might continue until a critical area A_c is extracted from the surface vesiculations. This behavior would be in contrast to the force versus length trends predicted for a tether formed by extracting area from the thermal undulations.

The tether force may reflect the microarchitectural properties in ways more subtle through the constant L_t^*. Since the differential area between the membrane leaflets is believed to contribute in part to the development of surface microvesiculations, those membranes which exhibit significant budding may also have a nontrivial L_t^* (43). Consequently, care should be taken when interpreting the response of tethers formed from vesicles with marked surface microvesiculations.

According to the analysis, as area is drawn from the thermal fluctuations to form a tether, the effective vesicle tension increases (Fig. 2 *B*). Due to the constant area constraint, the tension arising from expansion of molecular area is not included. For the small tensions considered in this model, the energy due to area expansion is much less than the thermal undulation term. As the tension increases, though, the area expansivity energy becomes larger than the undulation energy. The transition tension σ_{Trans} can be estimated by determining the tension for which the entropic and elastic stretching energies are equal (22,25): $\sigma_{Trans} \sim \kappa kT/k_c$. For a pure DOPC vesicle ($\kappa = 0.265$ N/m and $k_c = 8.5 \times 10^{-20}$ J (28)), σ_{Trans} is 0.84 mN/m. Because the initial tension influences the relation between tether force and tether length (Fig. 2 *B*), the exact tether length at which this transition tension is reached depends upon the initial effective tension.

The thermally driven surface undulations of the vesicle are approximated using a simple planar approach. This approach is valid for a spherical surface provided the amplitudes of the undulations are much smaller than the radius of the vesicle. Alternate models which employ either spherical harmonics or a coarse-grained approach may provide a more accurate

description of the surface undulations, especially those for vesicles with significant excess area (23,24). Of interest, theoretical studies have suggested if the vesicle has enough excess area, the effective tension may be <0 (24,44). This would have important implications for the physical actuality of the effective tension, a term often added as a Lagrange multiplier to enforce a constant area constraint (44). A ''negative tension'' might influence for example the vesicle microarchitecture. We also note that the presence of the tether will alter the overall characteristics of the surface undulations. The simple planar approximation employed, however, provides a basic description of the undulations of the vesicle surface as well as analytical relations for the dependence of the tether geometry on the tether force.

Previous work has considered how fluctuation-induced differential area dilation suppresses the mean-square amplitude of the bending undulations (11,45). Tether formation, however, imposes an additional area dilation field on the bilayer that could further suppress the surface undulations. Tether studies, especially at longer lengths, may provide a means to examine how differential area dilation affects the amplitude of surface undulations.

In summary, we have developed a model that provides a quantitative relation between force and tether conformation for a tether formed from an unaspirated lipid vesicle. According to the model, the thermal undulations of the vesicle surface can provide the excess area required for tether formation. The model captures both the increase in tether force with length and the decrease in tether radius observed experimentally (Fig. 3). Since the initial tension influences the extent of the undulations, the analysis indicates that the tether force is sensitive to these extraordinarily small tensions. Because these tensions are on the order of the resting tensions of cellular membranes, analyses of tether experiments can further our understanding of the role that thermally driven tensions play in biological processes.

We thank Gerbrand Koster, Enrique Munoz, and Anatoly Kolomeisky for providing valuable comments and discussions.

This work was supported by the National Science Foundation under grant No. 0114624.

REFERENCES

1. Bukman, D. J., J. H. Yao, and M. Wortis. 1996. Stability of cylindrical vesicles under axial tension. *Phys. Rev. E.* 54:5463–5468.
2. Waugh, R. E., J. Song, S. Svetina, and B. Zeks. 1992. Local and nonlocal curvature elasticity in bilayer membranes by tether formation from lecithin vesicles. *Biophys. J.* 61:974–982.
3. Waugh, R. E., and R. M. Hochmuth. 1987. Mechanical equilibrium of thick, hollow, liquid membrane cylinders. *Biophys. J.* 52:391–400.
4. Božič, B., S. Svetina, B. Žekš, and R. E. Waugh. 1992. Role of lamellar membrane structure in tether formation from bilayer vesicles. *Biophys. J.* 61:963–973.
5. Miao, L., U. Seifert, M. Wortis, and H. G. Dobereiner. 1994. Budding transitions of fluid-bilayer vesicles: The effect of area-difference elasticity. *Phys. Rev. E Stat. Phys. Plasmas Fluids Relat. Interdiscip. Topics.* 49:5389–5407.
6. Helfrich, W. 1974. Blocked lipid exchange in bilayers and its possible influence on the shape of vesicles. *Z. Naturforsch. [C].* 29C:510–515.
7. Evans, E. A. 1974. Bending resistance and chemically induced moments in membrane bilayers. *Biophys. J.* 14:923–931.
8. Raphael, R. M., and R. E. Waugh. 1996. Accelerated interleaflet transport of phosphatidylcholine molecules in membranes under deformation. *Biophys. J.* 71:1374–1388.
9. Svetina, S., B. Zeks, R. E. Waugh, and R. M. Raphael. 1998. Theoretical analysis of the effect of the transbilayer movement of phospholipid molecules on the dynamic behavior of a microtube pulled out of an aspirated vesicle. *Eur. Biophys. J.* 27:197–209.
10. Raphael, R. M., R. E. Waugh, S. Svetina, and B. Zeks. 2001. Fractional occurrence of defects in membranes and mechanically driven interleaflet phospholipid transport. *Phys. Rev. E Stat. Nonlin. Soft Matter Phys.* 64:051913.
11. Yeung, A., and E. Evans. 1995. Unexpected dynamics in shape fluctuations of bilayer vesicles. *J. Phys. II.* 5:1501–1523.
12. Hochmuth, R. M., N. Mohandas, E. E. Spaeth, J. R. Williamson, P. L. Blackshear Jr., and D. W. Johnson. 1972. Surface adhesion, deformation and detachment at low shear of red cells and white cells. *Trans. Am. Soc. Artif. Intern. Organs.* 18:325–334.
13. Sheetz, M. P. 2001. Cell control by membrane-cytoskeleton adhesion. *Nat. Rev. Mol. Cell Biol.* 2:392–396.
14. Hochmuth, R. M., and W. D. Marcus. 2002. Membrane tethers formed from blood cells with available area and determination of their adhesion energy. *Biophys. J.* 82:2964–2969.
15. Waugh, R. E., and R. G. Bauserman. 1995. Physical measurements of bilayer-skeletal separation forces. *Ann. Biomed. Eng.* 23:308–321.
16. Hwang, W. C., and R. E. Waugh. 1997. Energy of dissociation of lipid bilayer from the membrane skeleton of red blood cells. *Biophys. J.* 72: 2669–2678.
17. Hotani, H., and H. Miyamoto. 1990. Dynamic features of microtubules as visualized by dark-field microscopy. *Adv. Biophys.* 26:135–156.
18. Fygenson, D. K., J. F. Marko, and A. Libchaber. 1997. Mechanics of microtubule-based membrane extension. *Phys. Rev. Lett.* 79:4497–4500.
19. Roux, A., G. Cappello, J. Cartaud, J. Prost, B. Goud, and P. Bassereau. 2002. A minimal system allowing tubulation with molecular motors pulling on giant liposomes. *Proc. Natl. Acad. Sci. USA.* 99:5394–5399.
20. Koster, G., M. VanDuijn, B. Hofs, and M. Dogterom. 2003. Membrane tube formation from giant vesicles by dynamic association of motor proteins. *Proc. Natl. Acad. Sci. USA.* 100:15583–15588.
21. Upadhyaya, A., J. R. Chabot, A. Andreeva, A. Samadani, and A. van Oudenaarden. 2003. Probing polymerization forces by using actin-propelled lipid vesicles. *Proc. Natl. Acad. Sci. USA.* 100:4521–4526.
22. Evans, E., and W. Rawicz. 1990. Entropy-driven tension and bending elasticity in condensed-fluid membranes. *Phys. Rev. Lett.* 64:2094–2097.
23. Milner, S. T., and S. A. Safran. 1987. Dynamical fluctuations of droplet microemulsions and vesicles. *Phys. Rev. A.* 36:4371–4379.
24. Fournier, J. B., A. Ajdari, and L. Peliti. 2001. Effective-area elasticity and tension of micromanipulated membranes. *Phys. Rev. Lett.* 86: 4970–4973.
25. Helfrich, W. S. R.M. 1984. Undulations, steric interactions and cohesion of fluid membranes. *Il Nuovo Cimento.* 3D:137–151.
26. Discher, B. M., Y. Y. Won, D. S. Ege, J. C. Lee, F. S. Bates, D. E. Discher, and D. A. Hammer. 1999. Polymersomes: tough vesicles made from diblock copolymers. *Science.* 284:1143–1146.
27. Zhou, Y., and R. M. Raphael. 2005. Effect of salicylate on the elasticity, bending stiffness and strength of SOPC membranes. *Biophys. J.* 89: 1789–1801.
28. Rawicz, W., K. C. Olbrich, T. McIntosh, D. Needham, and E. Evans. 2000. Effect of chain length and unsaturation on elasticity of lipid bilayers. *Biophys. J.* 79:328–339.

29. Heinrich, V., B. Bozic, S. Svetina, and B. Zeks. 1999. Vesicle deformation by an axial load: from elongated shapes to tethered vesicles. *Biophys. J.* 76:2056–2071.

30. Heinrich, V., and R. E. Waugh. 1996. A piconewton force transducer and its application to measurement of the bending stiffness of phospholipid membranes. *Ann. Biomed. Eng.* 24:595–605.

31. Derenyi, I., F. Julicher, and J. Prost. 2002. Formation and interaction of membrane tubes. *Phys. Rev. Lett.* 88:238101.

32. Powers, T. R., G. Huber, and R. E. Goldstein. 2002. Fluid-membrane tethers: minimal surfaces and elastic boundary layers. *Phys. Rev. E.* 65: 041901.

33. Smith, A., E. Sackmann, and U. Seifert. 2004. Pulling tethers from adhered vesicles. *Phys. Rev. Lett.* 92:208101.

34. Hochmuth, R. M., J. Y. Shao, J. Dai, and M. P. Sheetz. 1996. Deformation and flow of membrane into tethers extracted from neuronal growth cones. *Biophys. J.* 70:358–369.

35. Helfrich, W. 1973. Elastic properties of lipid bilayers: theory and possible experiments. *Z. Naturforsch. [C].* 28:693–703.

36. Svetina, S., M. Brumen, and B. Zeks. 1985. Lipid bilayer elasticity and the bilayer couple interpretation of red-cell shape transformations and lysis. *Stud. Biophys.* 110:177–184.

37. Döbereiner, H. G., E. Evans, M. Kraus, U. Seifert, and M. Wortis. 1997. Mapping vesicle shapes into the phase diagram: a comparison of experiment and theory. *Phys. Rev. E Stat. Nonlin. Soft Matter Phys.* 55:4458–4474.

38. Helfrich, W. 1975. Out-of-plane fluctuations of lipid bilayers. *Z. Naturforsch. [C].* 30:841–842.

39. Palmer, M., R. Harris, C. Freytag, M. Kehoe, J. Tranum-Jensen, and S. Bhakdi. 1998. Assembly mechanism of the oligomeric streptolysin O pore: the early membrane lesion is lined by a free edge of the lipid membrane and is extended gradually during oligomerization. *EMBO J.* 17:1598–1605.

40. Upadhyaya, A., and M. P. Sheetz. 2004. Tension in tubulovesicular networks of Golgi and endoplasmic reticulum membranes. *Biophys. J.* 86:2923–2928.

41. Häckl, W., U. Seifert, and E. Sackmann. 1997. Effects of fully and partially solubilized amphiphiles on bilayer bending stiffness and temperature dependence of the effective tension of giant vesicles. *J. Phys. II.* 7:1141–1157.

42. Döbereiner, H. G., O. Selchow, and R. Lipowsky. 1999. Spontaneous curvature of fluid vesicles induced by trans-bilayer sugar asymmetry. *Eur. Biophys. J.* 28:174–178.

43. Iglic, A., and H. Hagerstrand. 1999. Amphiphile-induced spherical microexovesicle corresponds to an extreme local area difference between two monolayers of the membrane bilayer. *Med. Biol. Eng. Comput.* 37:125–129.

44. Seifert, U. 1995. The concept of effective tension for fluctuating vesicles. *Z. Phys. B: Condens. Matter.* 97:299–309.

45. Seifert, U. 1993. Curvature-induced lateral phase segregation in two-component vesicles. *Phys. Rev. Lett.* 70:1335–1338.